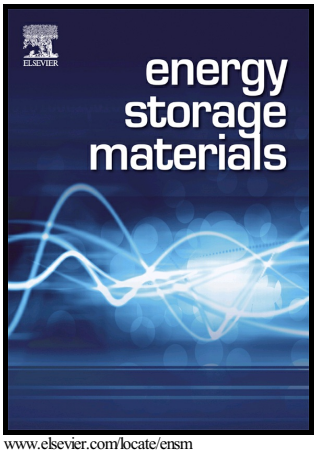

www.elsevier.com/locate/ensm

Enhanced electrochemical performance of hyperbranched poly(amidographene)

Kiran Babasaheb Dhopte, K. Mohanapriya, Neetu Jha, Parag R. Nemade

PII: S2405-8297(17)30368-9
DOI: https://doi.org/10.1016/j.ensm.2018.06.010
Reference: ENSM420

To appear in: *Energy Storage Materials*

Received date: 11 August 2017
Revised date: 4 June 2018
Accepted date: 10 June 2018

Cite this article as: Kiran Babasaheb Dhopte, K. Mohanapriya, Neetu Jha and Parag R. Nemade, Enhanced electrochemical performance of hyperbranched poly(amidographene), *Energy Storage Materials,* https://doi.org/10.1016/j.ensm.2018.06.010

Enhanced electrochemical performance of hyperbranched poly(amidographene)

Kiran Babasaheb Dhopte[a12], K. Mohanapriya[b1], Neetu Jha[a,b3], Parag R. Nemade[a,c4*]

[a]Department of Chemical Engineering, Institute of Chemical Technology, Nathalal Parekh Marg, Matunga, Mumbai Maharashtra, 400019, India

[b]Department of Physics, Institute of Chemical Technology, Nathalal Parekh Marg, Matunga, Mumbai Maharashtra, 400019, India

[c]Department of Oils, Oleochemicals and Surfactant Technology, Institute of Chemical Technology, Nathalal Parekh Marg, Mumbai, Maharashtra, 400 019, India

[*]Corresponding Author. Tel: +91 (22) 3361 2027, Fax: +91 (22) 3361 1020.

pr.nemade@ictmumbai.edu.in

Abstract

We report a facile route for the synthesis of hyperbranched polyamido-graphenes (HBP(A-G)) as non-metallic high capacity electrodes for charge storage in supercapacitors. HBP(A-G) were synthesized by Michael addition of polyamines, ethylene diamine (EDA), diethylene triamine (DETA), triethylene tetraamine (TETA), to acrylamide grafted graphene oxide, followed by reduction *in situ*. A 3D network of stiff graphene sheets connected by flexible polyamine chain was formed. Hyperbranching increased d-spacing and BET surface area of graphene stacks, which enhanced accessibility of sites for ion storage, and prevented restacking. HBP(A-G) electrodes displayed electric double layer capacitance behaviour with excellent specific capacitance. The charge storage

[1] KBD and KM have contributed equally to the work.
[2] 0000-0001-6723-837X
[3] 0000-0002-4540-1778
[4] 0000-0003-4680-1084

capacity of the electrodes increased with an increase in the amine chain length. Specific capacitance of electrodes containing HBP(TETA-G) was found to be 269 F g^{-1} in a symmetric two electrode electrochemical cell, using 1 M H_2SO_4 electrolyte at a current density of 1 A g^{-1} for voltage range of 0-1 V. An increase in the length of amine chains improved ion mobility, lowered equivalent distributed resistance and time constant of the electrodes. The time constant of HBP(TETA-G) capacitor was only 538 ms. Hydrophilic amine linkages on graphene backbone provided stability against electrode volume changes during charging and discharging and gave 89 % capacity retention over 10,000 cycles at 10 A g^{-1} current density for HBP(TETA-G) electrodes. HBP(A-G) electrodes demonstrated superior performance as electrodes for supercapacitors and has shown potential for use in other electrochemical applications.

Graphical abstract

Symmetric supercapacitor fabricated using hyperbranched poly(amidographene)s, synthesized via novel route by Michael addition of polyamines to acrylamide-grafted-graphene oxide followed by in situ reduction to graphene, gave high specific capacitance with good energy density.

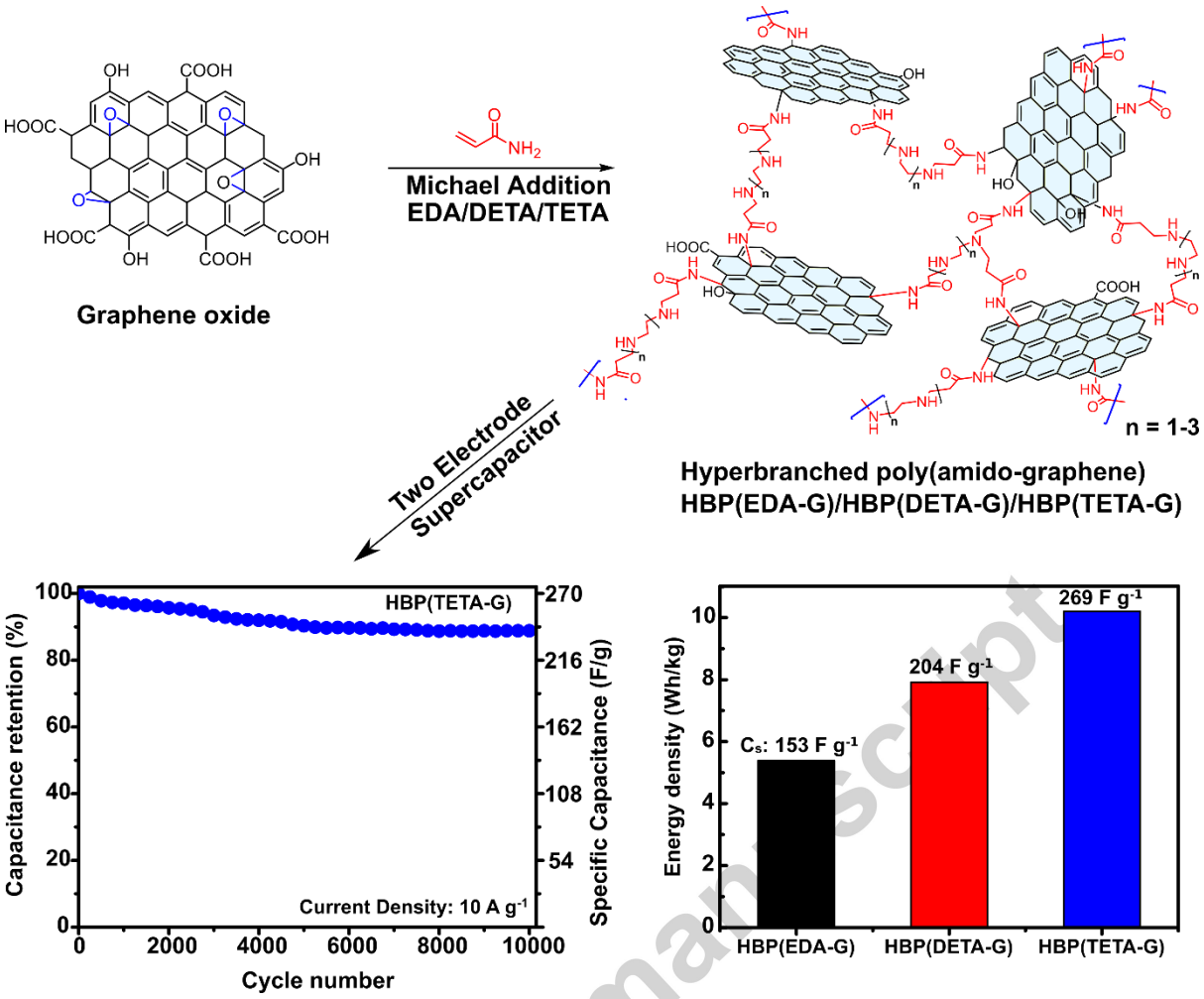

Keywords: Graphene oxide; Michael addition; hyperbranched poly(amido-graphene); supercapacitor;

Introduction

The recovery and storage of electrical energy is one of the most important challenges facing our society that is progressing in the direction of harnessing renewable energy, use of hybrid vehicles, etc. Batteries and electrochemical capacitors are most common energy storage technologies [1]. The cutting-edge battery technology is not adequate for powering these applications, mainly due to slow charge/discharge time, short life and high cost. Electrochemical

capacitors, also known as supercapacitors (SC) or ultracapacitors, combine the benefits of both, batteries and capacitors. Supercapacitors have much higher energy capacity than conventional capacitors, with similar rapid charge/discharge characteristics. Electric double layer capacitors (EDLC) are one type of SC containing high surface area material on which the charges accumulate. The other type of capacitor, known as pseudocapacitor, consists of conducting materials or those that undergo redox transformations [2]. Since pseudocapacitive materials have several times higher capacity, hybrid capacitators combing capacitive carbon based electrode with conductive or redox active materials have been in focus recently [3–7].

Graphene composed of sp^2 hybridized (2D) carbon atoms has driven great interest in the field due to unique properties such as high surface area, excellent thermal and mechanical stability, high conductivity, etc., which makes it an ideal material for EDLC [8,9]. One of the disadvantages of graphene is, its tendency to stack thereby decreasing the accessible surface area and the performance [10]. Studies on derivatives of graphene with conducting polymers such as polyethylenedioxythiophene [11,12], polyaniline [13,14], polypyrrole [15–17] are reported with the aim of decreasing the stacking tendencies.

Functionalization with hetero atoms like N-doped graphene [18,19], poly(ionic liquid) [20] are reported to enhance electrochemical properties of graphene based devices in addition to the increase in stability of graphene suspension. These approaches have conserved graphene stacks while increasing suspension stability, our approach is to disrupt graphene stacks through covalent functionalization with polymer, with the aim of exposing larger surface area for facilitating charge diffusion and storage. To that end, we grafted acrylamide on graphene oxide utilizing reactive epoxy groups giving GO-acrylamide (GO-A). Polyamine functionality is attached to GO-A through Michael addition. Acryl groups also react with secondary amines already attached to GO to create hyperbranched poly(amido-graphene oxide) derivatives. Amine functionalized graphene oxide is reduced *in situ* by annealing in presence of amines giving hyperbranched graphene (Figure 1). During

these transformations, covalently bound polyamine linkages are created between graphene sheets, which prevent restacking while increasing surface area and pore volume. Amine linkages also facilitate ion mobility and provide additional sites for charge storage.

Three amines with increasing chain length, ethylene diamine (EDA), diethylene triamine (DETA), and triethylene tetraamine (TETA), gave hyperbranched poly(ethylene diamido-graphene) (HBP(EDA-G)), hyperbranched poly(diethylene triamido-graphene) (HBP(DETA-G)), hyperbranched poly(triethylene tetraamido-graphene) (HBP(TETA-G)) respectively, which were characterized and then evaluated as electrodes for charge storage in supercapacitor. Chain length increases successively with EDA, DETA and TETA, which also increases the flexibility of crosslinks between graphene sheets. The volume of capacitor electrodes changes during charge and discharge cycles, therefore, an increase in flexibility is beneficial for increasing robustness and life of the electrode [21,22].

Results and Discussion

Elemental analysis of hyperbranched polyamido graphenes revealed the presence of nitrogen in HBP(A-G)s (ESI Table S1). A nitrogen loading of 11.4 % in HBP(EDA-G) was obtained, which increased marginally to 11.6 % in HBP(DETA-G) and to 16.7 % in HBP(TETA-G). The presence of large amount of nitrogen in elemental analysis indicates covalent bonding of nitrogenous functionalities to GO-A. The oxygen content in GO also decreased from 46 % to 18-12 % corresponding with an increase in nitrogen on the transformation to HBP(A-G).

FTIR spectra of GO showed prominent peaks at 3450 cm^{-1}, 1730 cm^{-1}, 1627 cm^{-1} and 1030 cm^{-1} corresponding to hydroxyl, carbonyl in carboxylic acid, olefin and epoxy groups respectively (Figure 2(a)). The increase in graphene character on reaction with acrylamide manifested as sharp decrease in intensity of broad –OH peak. New absorbance bands appeared at 3200 cm^{-1}, 1669 cm^{-1}, 1600 cm^{-1} and 967 cm^{-1} were attributed to amines (N-H), amides (O=C-N), aliphatic carbon (C-H) and olefin (C-H) groups respectively. The peak located at 1030 cm^{-1} in the spectra of GO attributed to

epoxy groups disappeared completely after the reaction. The intensity of olefin group peak increased in the GO-A spectra, which confirmed covalent amide functionalization of GO by acrylamide. Olefin functionality disappeared after Michael addition reaction. FTIR spectra of hyperbranched amines, shown in Figure 2(b), confirmed a decrease in the intensity of olefin peak alongwith the appearance of a broad peak at 3400-3442 cm^{-1} due to amines. Peaks attributed to aliphatic amines were observed at 1566 cm^{-1} and 1192 cm^{-1} in all hyperbranched poly(amido-graphene)s, which validate covalent addition of aliphatic polyamines to acrylamide functionalized GO. Further, the peaks due to oxygen functionalities either disappeared or were greatly reduced in intensity providing an evidence for increased graphene character.

Raman spectroscopy is an important tool to determine the chemical bonding, electronic variations, and disorder in carbonaceous materials. A single intense absorption G band peak at 1590 cm^{-1} corresponding to E_{2g} mode of sp^2 carbon atom is seen in the Raman spectra of natural graphite, while for graphene the G-band peak is found at 1580 cm^{-1}. (Figure 3) Prominent D band peak (1340-1350 cm^{-1}) corresponding to sp^3 hybridized carbon atoms is seen in addition to the G band peak at 1600-1610 cm^{-1} in the Raman spectra of graphene oxide (Figure 3). On functionalization by acrylamide, G band and D band peaks were found at 1603 cm^{-1} and 1354 cm^{-1} respectively, which were similar to the peak positions seen in the Raman spectra of GO. Since the grafting of acrylamide does not disturb the basic skeleton of parent GO sheet, the similarity is perhaps not surprising. The Raman spectra of HBP(EDA-G) shows an intense peak at 1339 cm^{-1} and a relatively less intense G band peak at 1598 cm^{-1}. The peaks continue to shift to a lower wavenumber in the spectra of HBP(DETA-G) and HBP(TETA-G). Increasing the I_D/I_G ratio from 0.92 in GO-A to 1.07-1.18 in the Raman spectra of HBP(A-G)s is due to the inclusion of nitrogen containing functional groups [23].

Grafting of acrylamide and subsequent hyperbranching due to *in-situ* Michael addition reaction on the surface of graphene oxide was confirmed by XPS analyses as shown in

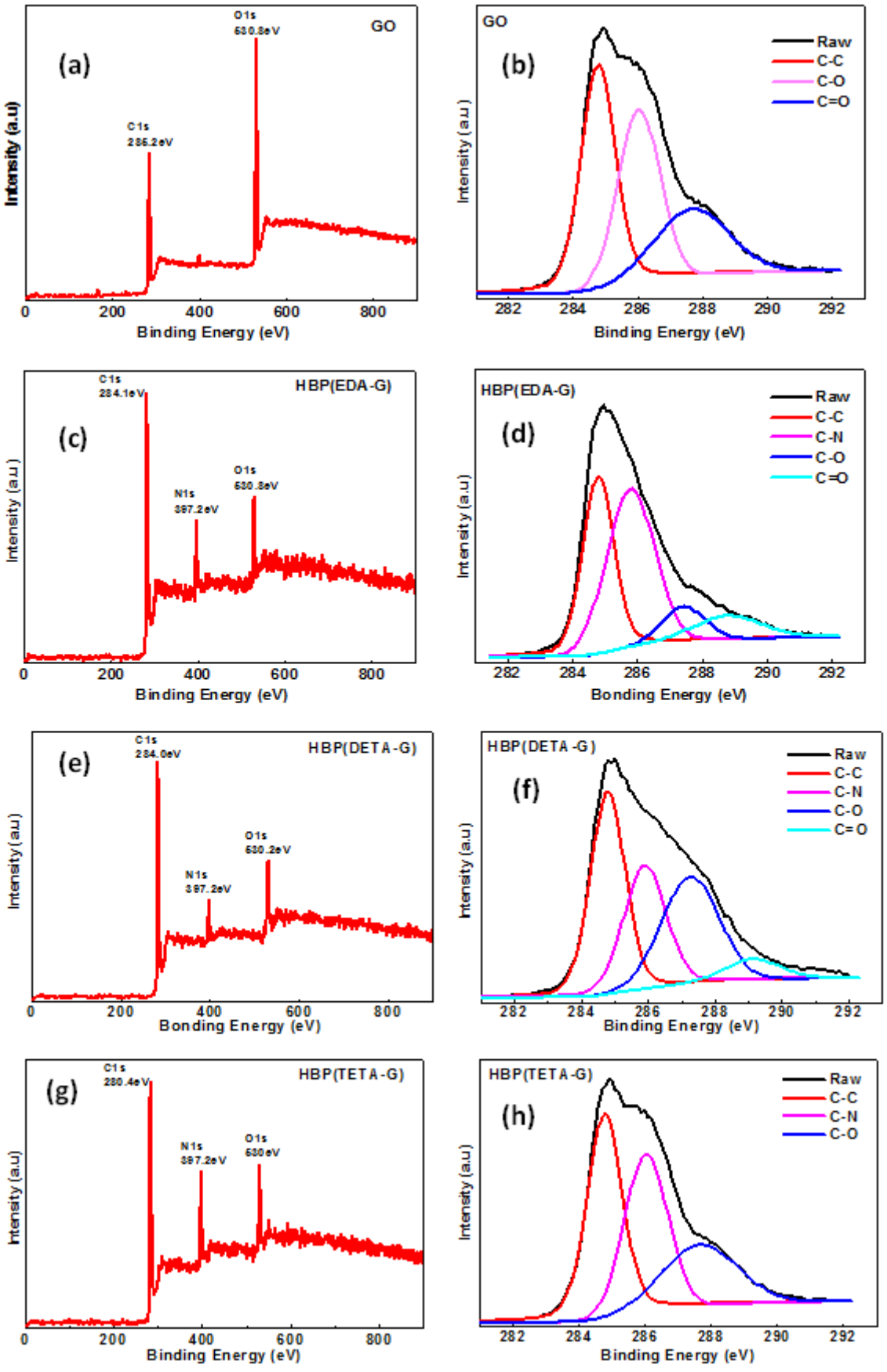
(a)
GO
O1s
530.8eV
C1s
286.2eV
Intensity (a.u)
Binding Energy (eV)
(b)
GO
Raw
C-C
C-O
C=O
Intensity (a.u)
Binding Energy (eV)
(c)
HBP(EDA-G)
C1s
284.1eV
N1s
397.2eV
O1s
530.8eV
Intensity (a.u)
Binding Energy (eV)
(d)
HBP(EDA-G)
Raw
C-C
C-N
C-O
C=O
Intensity (a.u)
Bonding Energy (eV)
(e)
HBP(DETA-G)
C1s
284.0eV
N1s
397.2eV
O1s
530.2eV
Intensity (a.u)
Bonding Energy (eV)
(f)
HBP(DETA-G)
Raw
C-C
C-N
C-O
C=O
Intensity (a.u)
Binding Energy (eV)
(g)
HBP(TETA-G)
C1s
280.4eV
N1s
397.2eV
O1s
530eV
Intensity (a.u)
Binding Energy (eV)
(h)
HBP(TETA-G)
Raw
C-C
C-N
C-O
Intensity (a.u)
Binding Energy (eV)

Figure 4. Survey XPS spectra of GO revealed two peaks attributed to C1s and O1s spectra.

The survey spectrum of HBP(A-G) revealed an additional N1s peak. The intensity of O1s peak decreased on transformation to HBP(A-G) indicating reduction of GO. The elemental composition obtained from XPS was in agreement with that obtained using elemental analysis. C1s spectrum of GO was deconvoluted in to three peaks corresponding to: (a) C-C, C=C, C-H groups (284.5 eV); (b) C-OH groups (286.9 eV); and (c) O=C-OH groups (288.6 eV). The peak corresponding to epoxy group overlaps with that of hydroxyl groups at 286.9 eV. On Michael addition of polyamines, a new peak attributed to C-N linkage appeared in the spectra of HBP(A-G) (285.9 eV). The intensity of this peak indicated the extent of addition of nitrogen functionalities to graphene oxide. As the length of amine chain in HBP(A-G) increased, the intensity of peaks attributed to C-N and C-C linkages increased (

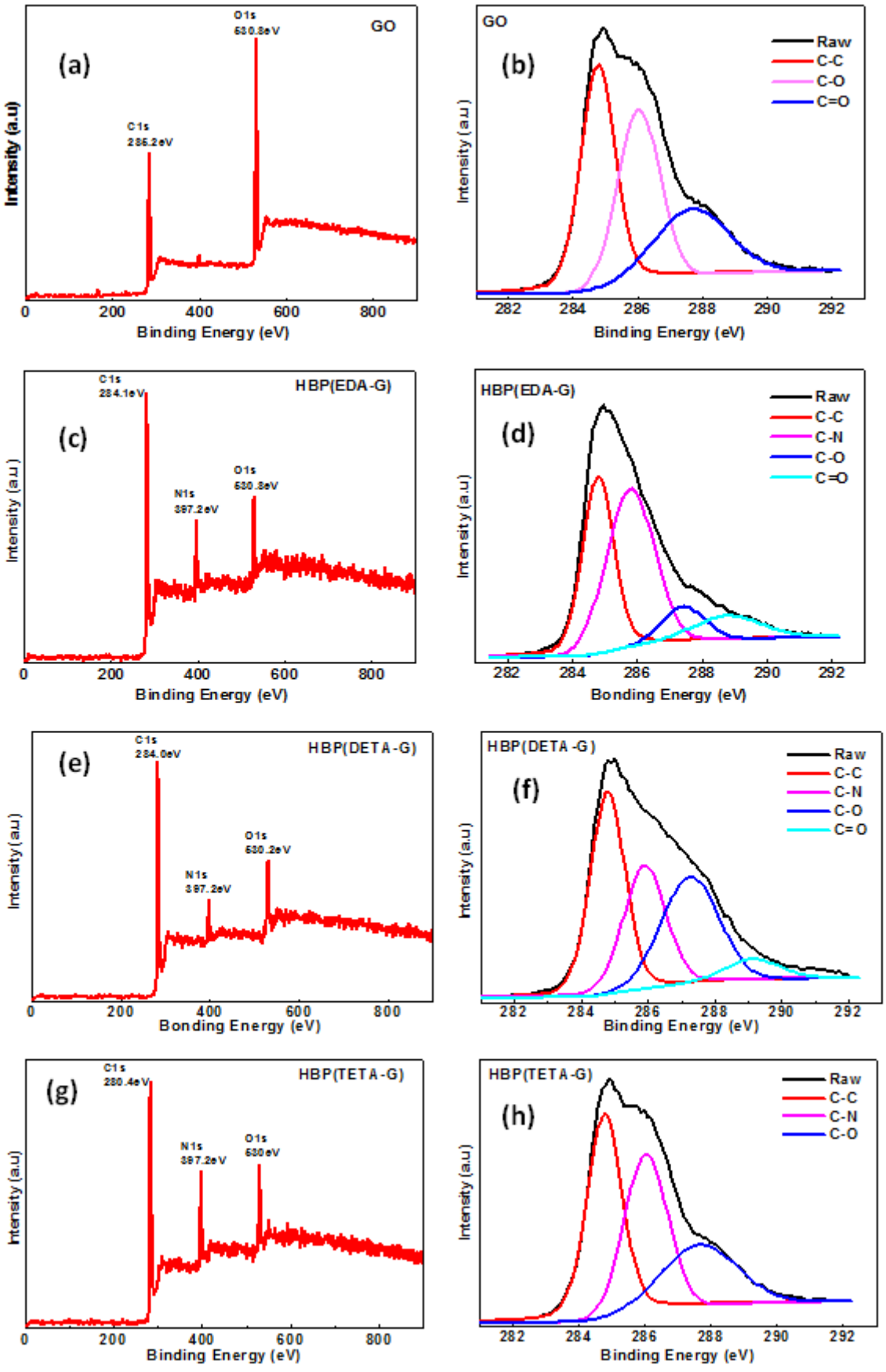
(a)
GO
O1s
530.8eV
C1s
286.2eV
Intensity (a.u)
Binding Energy (eV)
(b)
GO
Raw
C-C
C-O
C=O
Intensity (a.u)
Binding Energy (eV)
(c)
HBP(EDA-G)
C1s
284.1eV
N1s
397.2eV
O1s
530.8eV
Intensity (a.u)
Binding Energy (eV)
(d)
HBP(EDA-G)
Raw
C-C
C-N
C-O
C=O
Intensity (a.u)
Bonding Energy (eV)
(e)
HBP(DETA-G)
C1s
284.0eV
N1s
397.2eV
O1s
530.2eV
Intensity (a.u)
Bonding Energy (eV)
(f)
HBP(DETA-G)
Raw
C-C
C-N
C-O
C=O
Intensity (a.u)
Binding Energy (eV)
(g)
HBP(TETA-G)
C1s
280.4eV
N1s
397.2eV
O1s
530eV
Intensity (a.u)
Binding Energy (eV)
(h)
HBP(TETA-G)
Raw
C-C
C-N
C-O
Intensity (a.u)
Binding Energy (eV)

Figure 4f and

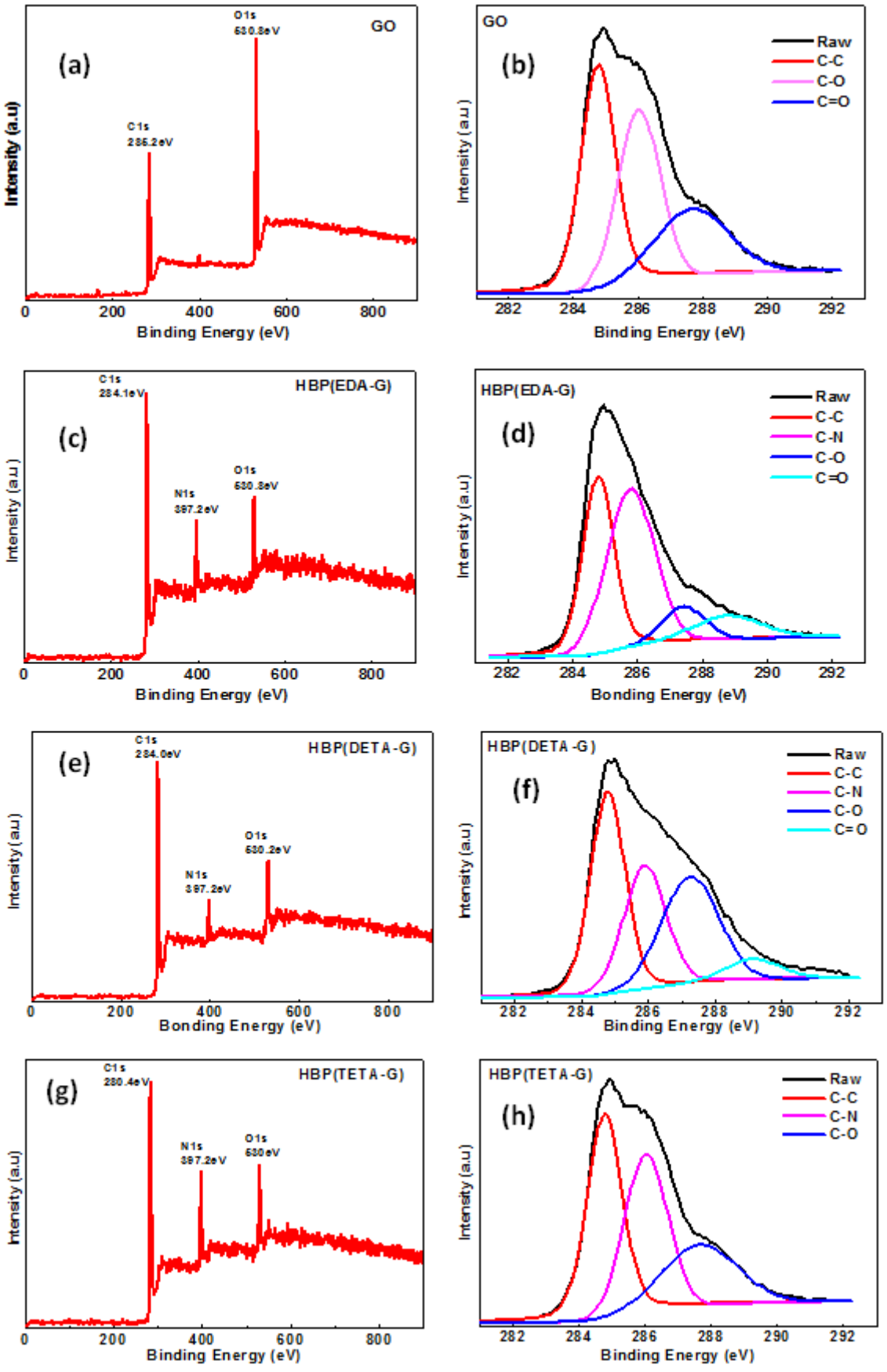
(a)
GO
O1s
530.8eV
C1s
286.2eV
Intensity (a.u)
Binding Energy (eV)
(b)
GO
Raw
C-C
C-O
C=O
Intensity (a.u)
Binding Energy (eV)
(c)
HBP(EDA-G)
C1s
284.1eV
N1s
397.2eV
O1s
530.8eV
Intensity (a.u)
Binding Energy (eV)
(d)
HBP(EDA-G)
Raw
C-C
C-N
C-O
C=O
Intensity (a.u)
Bonding Energy (eV)
(e)
HBP(DETA-G)
C1s
284.0eV
N1s
397.2eV
O1s
530.2eV
Intensity (a.u)
Bonding Energy (eV)
(f)
HBP(DETA-G)
Raw
C-C
C-N
C-O
C=O
Intensity (a.u)
Binding Energy (eV)
(g)
HBP(TETA-G)
C1s
280.4eV
N1s
397.2eV
O1s
530eV
Intensity (a.u)
Binding Energy (eV)
(h)
HBP(TETA-G)
Raw
C-C
C-N
C-O
Intensity (a.u)
Binding Energy (eV)

Figure 4h) as well [24]. Two peaks, at 399 eV and 402.1 eV attributed to H-N-C and O=C-N groups respectively, can be seen in the N1s spectrum of the materials (Figure S1) [25].

X-ray diffraction (XRD) analysis revealed the distortion of the lamellar structure of graphene oxide stack after the insertion of acrylamide functionality on GO surface (Figure 5). XRD spectra of GO showed a sharp intense peak at 2θ = 9.8° with an interlayer spacing of 0.80 nm. In the XRD spectra of GO-A, the peak was shifted to higher angle (2θ = 10.1°), was broader and less intense. The broad nature of primary peak along with a decrease in intensity implies disruption of GO stacks due to the addition of acrylamide groups. Additional functionality led to a decrease in the interlayer spacing (0.88 nm). After GO-A synthesis, the combination of Michael addition and *in situ* reduction resulted in the disappearance of parent GO peak along and appearance of broad peaks in the spectra of HBP(EDA-G) at approx. 24.2° with an interlayer spacing of 0.36 nm, which can be attributed to the graphene stacks [25]. The interlayer spacing increased as the length of aliphatic chain increased in HBP(DETA-G), however, the peak height decreased. The primary peak corresponding to graphene disappeared completely, when the length of polyamine chain was increased further in HBP(TETA-G). The amplitude of primary peaks decreased with increasing chain length of amine used during amide functionalization implying that the hyperbranched amidation at high temperature disrupted lamellar structure of graphene. Crosslinking between graphene oxide sheets due to polyamine grafting may have restricted aggregation, resulting in the exfoliation of GO [26]. BET analysis revealed pore distribution within the range of 2-40 nm with high concentration of pores with < 4 nm diameter (ESI Figure S2(b)). BET surface area of HBP(EDA-G) was 91.5 m^2/g corresponding to pore volume of 0.08 $m^3\ g^{-1}$. HBP(DETA-G) had a lower surface area of 84.7 $m^2\ g^{-1}$ with marginally higher pore volume of 0.1 m^3/g. HBP(TETA-G) exhibited highest surface area of 100.1 $m^2\ g^{-1}$ with 0.14 $m^2\ g^{-1}$ pore volume. Thus, HBP(TETA-G) showed highly porous structure with abundant amine functionalities facilitating charge storage and mobility [27].

Thermogravimetric analyses (TGA) were carried out in N_2 atmosphere to determine the variation in the characteristics of the carbon nanomaterial after various transformations (ESI Figure S3). GO lost 60 % weight between 100 to 210 °C, due to the loss of free moisture and due to the loss of oxygen functionalities such as epoxy groups on the GO surface. A gradual weight loss (30 %) between 130 to 220 °C can be seen in the TGA curve of GO-A. Epoxy rings in GO are opened during acrylamide grafting to give GO-A. Consequently, the thermal stability is improved. On heating GO-A to 800 °C, a residue of about 45 % was obtained. Michael addition of polyamines to GO-A further enhanced the thermal stability of the carbon nanomaterial. HBP(EDA-G), HBP(DETA-G) and HBP(TETA-G) lost less than 15 % weight when the samples were heated to 250 °C. Gradual weight loss was observed on heating HBP(EDA-G) and HBP(DETA-G) to 800 °C, giving 63 % and 58 % residue respectively. In case of HBP(TETA-G), about 33 % weight loss was obtained between 250 to 430 °C and heating further to 800 °C resulted in 45 % residual mass. The improved thermal stability of hyperbranched graphenes confirmed both covalent bonding of polyamines to GO sheets and an increase in graphene character.

The electrochemical performance of HBP(EDA-G), HPB-(DETA-G) and HBP(TETA-G) electrodes was evaluated in a symmetric two electrode electrochemical cell, with 1 M H_2SO_4 as electrolyte for voltage range of 0-1 V. Cyclic voltammograms (CV) of HBP(EDA-G), HBP(DETA-G) and HBP(TETA) electrodes at the scan rate of 100 mV s^{-1} showed near rectangular curves revealing electric double layer capacitor (EDLC) behaviour (Figure 6 (a)). Amine functionalities do not seem to undergo redox reactions. Hence, the change in the electrochemical performance was directly associated with change in graphene structure [28]. An increase in current with increasing amine functionality indicates faster ion movement. Detailed CV curves of HBP(EDA-G), HPB-(DETA-G) and HBP(TETA-G) at scan rates between 30-200 mV s^{-1} are presented in supporting information (ESI, Figures S4-S6). All samples displayed near rectangular-shape even at high scan rate (200 mV s^{-1}) denoting efficient electrolyte ion transport through the electrodes.

Figure 6 (b) gives galvanostatic charge/discharge (CD) curves for HBP(EDA-G), HBP(DETA-G) and HBP(TETA-G) devices at current density of 1 A/g. The CD curves exhibit triangular shape indicating EDLC behaviour. The excellent electrochemical reversibility of the materials was reflected in the symmetric nature of the charge-discharge curves. Detailed CD curves at different current densities from 1 to 10 A g^{-1} were measured to understand the feasibility of the electrode materials in supercapacitor (ESI, Figures S7-S9). Specific capacitance (C_s) was calculated from the discharge curves using equation (1) [29].

$$C_s = 4 \cdot \frac{I \times \Delta t}{m \times \Delta V} \quad (1)$$

Where, I is the constant current applied, Δt is the total discharge time, m is the mass of the two electrodes and ΔV is the voltage window after the IR drop of discharge curves. HBP(TETA-G) displayed highest specific capacitance of 269 F g^{-1} at a current density of 1 A g^{-1} among the materials studied. Specific capacitance of HBP(DETA-G) and HBP(EDA-G) was lower by 24 % and 43 % respectively. Specific capacitance depends on the electrode material, electrolyte, wettability of electrode by the electrolyte, conductivity and porosity of the electrode [30]. It is important to note that the BET surface area does not necessarily reflect the actual accessible sites the electrolyte ions can reside on. The pore size should be slightly higher than the size of electrolyte ions to get higher electroactive surface area. Presence of amine functionalities increased the number of charge storage sites and improved the surface wettability for aqueous electrolytes, aiding diffusion and migration of electrolyte ions through poly(amido-graphene) network during charging and discharging [31]. Figure 6 (c) shows that specific capacitance decreased on increasing current density from 1 to 10 A g^{-1}. On increasing the current density 10-fold, only 18.5 % drop in specific capacitance of HBP(TETA-G) was observed. The capacitance was also estimated based on the area under the CD curves and average difference in the capacitance obtained was about 2 % (Figure S10).

Electrochemical impedance spectroscopy was carried out to understand the ion transport kinetics in the electrodes for the frequency range of 100 KHz to 0.01 Hz. Figure 6 (d) shows the

Nyquist plots and the curves fitted to an equivalent circuit (given in the inset) for HBP(EDA-G), HBP(DETA-G) and HBP(TETA-G) based electrodes. The parameters, total cell resistance (R_{cell}), equivalent series resistance (ESR), charge transfer resistance (R_{CT}), and equivalent distributed resistance, obtained from fitting the curve to the equivalent circuit are presented in the table in inset of Figure 6d. The first intercept on real axis in the high-frequency region is defined as the equivalent series resistance. Lower ESR value indicates high conductivity of the electrode material and good electrical contact at the electrode-current collector interface. The ESR values were found to be almost the same for all three materials. The total cell resistance was obtained by extrapolating the linear portion of the curve in the low frequency region to the real axis. R_{cell} of HBP(EDA-G), HBP(DETA-G) and HBP(TETA-G) electrodes was found to be 2.9 Ω, 2.1 Ω and 1.6 Ω respectively. R_{ct} was calculated from the diameter of semicircle in the high to medium frequency region. R_{ct} of HBP(EDA-G), HBP(DETA-G) and HBP(TETA-G) electrodes was found to be 0.15 Ω, 0.11 Ω and 0.11 Ω respectively. EDR was calculated by subtracting R_{CT} and ESR from R_{cell}. HBP(TETA-G) electrode showed lowest EDR of 0.72 Ω. The EDR of HBP(EDA-G) and HBP(DETA-G) electrodes was 178 % and 70 % higher than that of HBP(TETA-G) respectively. Lower R_{CT} and EDR signifies low intrinsic and interfacial resistance with efficient charge mobility that leads to better performance [32].

Figure 6 (e) shows the dependence of phase angle on the frequency for HBP(EDA-G), HBP(DETA-G) and HBP(TETA-G) electrodes. The time constant τ_0 was calculated using the equation (2) [33]

$$\tau_0 = {}^{1}/_{f_0} \qquad (2)$$

Where, f_0 is the characteristic frequency (at the phase angle of -45°) and τ_0 represents the minimum time required to discharge all the stored energy from the sample with minimum 50% efficiency. The lower time constant affording faster charge-discharge rate is a desirable property in supercapacitors. τ_o of HBP(TETA-G) (538 ms) electrode was lower than that of the electrodes containing HBP(DETA-G) (973 ms) and HBP(EDA-G) (848 ms). Although, graphene has high electrical conductivity, it is not

hydrophilic. Reduced graphene oxide with a few oxygen-containing groups attached on the edges aid in electrolyte mobility through the graphene domains. Addition of amine chains to the edges improves hydrophilicity and lowers resistance, aiding charge migration through poly(amido-graphene) network during charging and discharging [31]. Higher degree of exfoliation, larger pore volume and lower EDR in HBP(TETA-G) than other polyamine analogues gave electrode with higher specific capacitance and lower time constant.

The stability of HBP(TETA-G) electrode was evaluated by performing CD measurements between 0-1 V at current density of 10 A g^{-1} for 10,000 cycles in 1 M H_2SO_4 as shown in Figure 6 (f). HBP(TETA-G) electrode retained 89 % of its initial capacitance after 10,000 cycles. Hyperbranched poly(amido-graphene) network shows excellent resilience to structural stress during rapid charge-discharge cycling denoting efficient intake, storage and discharge of electrolyte ions during charging and discharging.

Figure 7 presents the Ragone plot of the samples, showing the relationship between the energy density and power density. The energy density (E) and power density (P) were calculated from the discharge curves according to the equation (3) and equation (4), where C_s is the specific capacitance, V is the applied voltage and t is the discharge time respectively [29].

$$E = \frac{1}{2}\left(\frac{C_S}{4}\right)V^2 \quad (3)$$

$$P = \frac{E}{t} \quad (4)$$

HBP(TETA-G) electrodes had higher specific energy density (9.3 Wh kg^{-1}) and power density (504 W kg^{-1}) than those with HBP(DETA-G) (7.1 Wh kg^{-1}) and HBP(EDA-G) (5.3 Wh kg^{-1}). The power density increases to 5262 W kg^{-1} when the energy density decreased to 7.6 Wh kg^{-1} and the retention rate is 82%. HBP(TETA-G) electrode material showed excellent rate capability and energy density, which can be increased further for practical applications by increasing the operating potential window through use of non-aqueous electrolytes.

Conclusion

In conclusion, a novel route is proposed for functionalization of graphene oxide by the insertion of aliphatic amine groups, EDA, DETA and TETA, via Michael addition giving hyperbranched structure. Aliphatic amine groups create linkage between GO sheets, while reducing GO to graphene simultaneously. The grafting of covalently bonded hyperbranched polyamine chains resulted in increased exfoliation of few-layered graphene. The highest specific capacitance of 269 F g^{-1} was obtained for HBP(TETA-G) using 1 M H_2SO_4 electrolyte between the voltage range of 0-1 V with excellent stability. This performance is attributed to excellent wettability of HBP(TETA-G), high pore volume and high surface area due to the presence of amine linkages on graphene backbone that improve charge mobility and provide stability during charge discharge cycles. This architecture can also be employed for fabricating high-performance electrodes for batteries and other electronic devices, in catalysts, adsorbents, biomedical applications, etc.

Experimental

Natural graphite powder (325 mesh) was purchased from Alfa Aesar. Potassium permanganate ($KMnO_4$), sulphuric acid (H_2SO_4), sodium nitrite ($NaNO_3$), hydrogen peroxide (30 % H_2O_2), hydrochloric acid (35 % HCl) acquired from S. D. Fine Chem. Ltd., Mumbai. Aliphatic amines, ethylene diamine (EDA), diethylene triamine (DETA) and triethylene tetraamine (TETA) were purchased from Loba Chemicals, acrylamide was purchased from Sigma Aldrich. The chemicals were used as received without any further purification.

Exprimental procedure for synthesis of graphene oxide:

Sodium nitrate ($NaNO_3$, 500 mg), concentrated sulphuric acid (H_2SO_4, 23 mL) and natural graphite powder (1 g) were mixed in to 500 ml round bottom flask maintained at 5 °C, subsequently, potassium permanganate ($KMnO_4$, 7 g) was slowly added to the RBF under continuous stirring. The

reaction mixture was stirred for about 2 h. The reaction mass was diluted with water (296 ml). 10 % H_2O_2 (10 ml) to bleach the reaction mass, and was left overnight for settling and then filtered. The residue was washed 4 times alternately with DI water and HCl; and again washed with DI water several times to remove traces of acid. GO, so obtained was suspended in DI water by sonication at 10 °C for 60 min and then dried under vacuum.

Experimental procedure for synthesis of GO-A:

GO-monoacrylamide (GO-A) was synthesized by reaction of acrylamide with GO in a three necked round bottom flask maintained under nitrogen atmosphere equipped with a water condenser in an oil bath. 100 mg GO was dispersed in 150 ml of DI water using sonication. This suspension was added to 15 ml solution of acrylamide in water, and heated to 60 °C under N_2 atmosphere for 24 h. GO-A, so obtained, was isolated from the reaction mixture by repeated centrifugation and washing with water. Finally the product was vacuum dried at 60 °C for 12 h [24].

Experimental procedure for synthesis of hyperbranched amido-graphene: (HBAG)

Hyperbranched amido-graphene (HBAG) was synthesized by Michael addition of ethylene diamine (EDA), diethylene triamine (DETA) or triethlylene tetraamine (TETA) to GO-A. In typical procedure, GO-A (100 mg) was dispersed in 100 ml anhydrous methanol by sonication and was cooled to 0 °C temperature. 5 ml of respective amine, EDA, DETA or TETA was added dropwise to the solution under constant stirring for 1 h. Subsequently, the temperature was raised to 30 °C and was stirred for another 2 h. Methanol was evaporated under vacuum. The residue was then heated to 100 °C for 2 h followed by heating at 120 °C for another 2 h. The reaction mass was washed with DI water multiple times to remove unreacted amine followed by washing with methanol and then dried under reduced pressure to give HBAG.

Characterization techniques

The extent of amination on the surface of GO was estimated using CHNSO analysis (Thermo Finnigan, FLASH EA 1112). Covalent functionalization of GO was confirmed by infrared spectroscopy

(VERTEX 80V, Bruker) and Raman spectroscopy (HR-800, Horiba Scientific). Nature of N-atom bonding on graphene oxide surface was determined using X-ray photoelectron spectroscopy (XPS) analyses performed on PHI 5000 Versa probe II instrument equipped with monochromatic Al Kα X-ray source. The change in stacking in GO due functionalization was estimated from X-ray diffraction (XRD, Bruker X- ray Diffractometer, D8-Adavance) using monochromatised Cu Kα radiation (λ = 1.5406 Å). Sheet structure and stacking in HBAG was imaged using scanning electron microscopy. The surface area was measured with BET sorptometer (BET-201A) using nitrogen adsorption and desorption isotherms after degasification at 120 °C temperature for 2 hrs.

Electrochemical measurements

Supercapacitor electrodes with an effective area of 0.785 cm^2 were prepared by drop-casting sonicated suspension of HBAG in ethanol (3 g/L) on graphite paper followed by drying at room temperature. The increase in mass of the graphite sheet gave the exact amount of HBAG deposited on the electrode. Supercapacitor was assembled in a Swagelok cell using two identical HBAG coated electrodes separated by filter paper. Electrochemical measurements such as cyclic voltammetry, galvanostatic charge/discharge analysis, electrochemical impedance spectroscopy (EIS) were carried out using two electrode method on an electrochemical workstation (μAutolab Type III, Metrohm) with 1 N H_2SO_4 as electrolyte between 0-1 V. EIS curves were fitted to circuit model using Nova 1.11 software.

Electronic Supplementary Information

Electronic supplementary information attached lists elemental analysis of various HBP(A-G), deconvoluted XPS N1s spectra of HBP(A-G), BET adsorption desorption isotherms and pore size distribution-pore volume analysis, TGA analysis of GO, GO-A, and HBP(A-G), CV curves for scan rates from 30-200 mV/s and charge-discharge curves at current densities ranging from 1-10 A/g for HBP(A-G).

Acknowledgement

We are thankful to the University Grants Commission of the Government of India for support under UGC-BSR Fellowships and UGC-Networking Resource Centre. We would also like to acknowledge assistance provided by Sophisticated Analytical Instrumentation Facility, IIT Bombay and Centre for Nanotechnology, University of Mumbai for analytical support.

References

[1] B.E. Conway, Electrochemical Supercapacitors - Scientific Fundamentals and | B. E. Conway | Springer, 1st ed., Springer US, New York, 1999. http://www.springer.com/in/book/9780306457364 (accessed July 5, 2017).
[2] P. Simon, Y. Gogotsi, Materials for electrochemical capacitors, Nat. Mater. 7 (2008) 845–854. doi:10.1038/nmat2297.
[3] A.D. Fabio, A. Giorgi, M. Mastragostino, F. Soavi, Carbon-Poly(3-methylthiophene) Hybrid Supercapacitors, J. Electrochem. Soc. 148 (2001) A845–A850. doi:10.1149/1.1380254.
[4] J.H. Park, O.O. Park, Hybrid electrochemical capacitors based on polyaniline and activated carbon electrodes, J. Power Sources. 111 (2002) 185–190. doi:10.1016/S0378-7753(02)00304-X.
[5] P. Gómez-Romero, M. Chojak, K. Cuentas-Gallegos, J.A. Asensio, P.J. Kulesza, N. Casañ-Pastor, M. Lira-Cantú, Hybrid organic–inorganic nanocomposite materials for application in solid state electrochemical supercapacitors, Electrochem. Commun. 5 (2003) 149–153. doi:10.1016/S1388-2481(03)00010-9.
[6] X. Lang, A. Hirata, T. Fujita, M. Chen, Nanoporous metal/oxide hybrid electrodes for electrochemical supercapacitors, Nat. Nanotechnol. 6 (2011) 232–236. doi:10.1038/nnano.2011.13.
[7] S. Chen, J. Zhu, X. Wu, Q. Han, X. Wang, Graphene Oxide−MnO2 Nanocomposites for Supercapacitors, ACS Nano. 4 (2010) 2822–2830. doi:10.1021/nn901311t.
[8] C.N.R. Rao, A.K. Sood, K.S. Subrahmanyam, A. Govindaraj, Graphene: The New Two-Dimensional Nanomaterial, Angew. Chem. Int. Ed. 48 (2009) 7752–7777. doi:10.1002/anie.200901678.
[9] Z. Weng, Y. Su, D.-W. Wang, F. Li, J. Du, H.-M. Cheng, Graphene-Cellulose Paper Flexible Supercapacitors, Adv. Energy Mater. 1 (2011) 917–922. doi:10.1002/aenm.201100312.
[10] M.D. Stoller, S. Park, Y. Zhu, J. An, R.S. Ruoff, Graphene-Based Ultracapacitors, Nano Lett. 8 (2008) 3498–3502. doi:10.1021/nl802558y.
[11] F. Alvi, M.K. Ram, P.A. Basnayaka, E. Stefanakos, Y. Goswami, A. Kumar, Graphene–polyethylenedioxythiophene conducting polymer nanocomposite based supercapacitor, Electrochimica Acta. 56 (2011) 9406–9412. doi:10.1016/j.electacta.2011.08.024.
[12] T.T. Tung, T.Y. Kim, J.P. Shim, W.S. Yang, H. Kim, K.S. Suh, Poly(ionic liquid)-stabilized graphene sheets and their hybrid with poly(3,4-ethylenedioxythiophene), Org. Electron. 12 (2011) 2215–2224. doi:10.1016/j.orgel.2011.09.012.

[13] Q. Wu, Y. Xu, Z. Yao, A. Liu, G. Shi, Supercapacitors Based on Flexible Graphene/Polyaniline Nanofiber Composite Films, ACS Nano. 4 (2010) 1963–1970. doi:10.1021/nn1000035.
[14] J. Xu, K. Wang, S.-Z. Zu, B.-H. Han, Z. Wei, Hierarchical Nanocomposites of Polyaniline Nanowire Arrays on Graphene Oxide Sheets with Synergistic Effect for Energy Storage, ACS Nano. 4 (2010) 5019–5026. doi:10.1021/nn1006539.
[15] M. Deng, X. Yang, M. Silke, W. Qiu, M. Xu, G. Borghs, H. Chen, Electrochemical deposition of polypyrrole/graphene oxide composite on microelectrodes towards tuning the electrochemical properties of neural probes, Sens. Actuators B Chem. 158 (2011) 176–184. doi:10.1016/j.snb.2011.05.062.
[16] S. Konwer, R. Boruah, S.K. Dolui, Studies on Conducting Polypyrrole/Graphene Oxide Composites as Supercapacitor Electrode, J. Electron. Mater. 40 (2011) 2248. doi:10.1007/s11664-011-1749-z.
[17] C. Zhu, J. Zhai, D. Wen, S. Dong, Graphene oxide/ polypyrrole nanocomposites: one-step electrochemical doping, coating and synergistic effect for energy storage, J. Mater. Chem. 22 (2012) 6300–6306. doi:10.1039/C2JM16699B.
[18] B.-H. Jeong, E.M.V. Hoek, Y. Yan, A. Subramani, X. Huang, G. Hurwitz, A.K. Ghosh, A. Jawor, Interfacial polymerization of thin film nanocomposites: A new concept for reverse osmosis membranes, J. Membr. Sci. 294 (2007) 1–7. doi:10.1016/j.memsci.2007.02.025.
[19] B. Jiang, C. Tian, L. Wang, L. Sun, C. Chen, X. Nong, Y. Qiao, H. Fu, Highly concentrated, stable nitrogen-doped graphene for supercapacitors: Simultaneous doping and reduction, Appl. Surf. Sci. 258 (2012) 3438–3443. doi:10.1016/j.apsusc.2011.11.091.
[20] T.Y. Kim, H.W. Lee, M. Stoller, D.R. Dreyer, C.W. Bielawski, R.S. Ruoff, K.S. Suh, High-Performance Supercapacitors Based on Poly(ionic liquid)-Modified Graphene Electrodes, ACS Nano. 5 (2011) 436–442. doi:10.1021/nn101968p.
[21] B.R. Duan, Q. Cao, Hierarchically porous Co3O4 film prepared by hydrothermal synthesis method based on colloidal crystal template for supercapacitor application, Electrochimica Acta. 64 (2012) 154–161. doi:10.1016/j.electacta.2012.01.004.
[22] X. Chen, X. Chen, F. Zhang, Z. Yang, S. Huang, One-pot hydrothermal synthesis of reduced graphene oxide/carbon nanotube/α-Ni(OH)2 composites for high performance electrochemical supercapacitor, J. Power Sources. 243 (2013) 555–561. doi:10.1016/j.jpowsour.2013.04.076.
[23] Z.-Y. Sui, Y. Cui, J.-H. Zhu, B.-H. Han, Preparation of Three-Dimensional Graphene Oxide–Polyethylenimine Porous Materials as Dye and Gas Adsorbents, ACS Appl. Mater. Interfaces. 5 (2013) 9172–9179. doi:10.1021/am402661t.
[24] Y.-L. Huang, H.-W. Tien, C.-C.M. Ma, S.-Y. Yang, S.-Y. Wu, H.-Y. Liu, Y.-W. Mai, Effect of extended polymer chains on properties of transparent graphene nanosheets conductive film, J. Mater. Chem. 21 (2011) 18236–18241. doi:10.1039/C1JM13790E.
[25] B. Yuan, C. Bao, L. Song, N. Hong, K.M. Liew, Y. Hu, Preparation of functionalized graphene oxide/polypropylene nanocomposite with significantly improved thermal stability and studies on the crystallization behavior and mechanical properties, Chem. Eng. J. 237 (2014) 411–420. doi:10.1016/j.cej.2013.10.030.
[26] L. Hu, Z. Yang, L. Cui, Y. Li, H.H. Ngo, Y. Wang, Q. Wei, H. Ma, L. Yan, B. Du, Fabrication of hyperbranched polyamine functionalized graphene for high-efficiency removal of Pb(II) and methylene blue, Chem. Eng. J. 287 (2016) 545–556. doi:10.1016/j.cej.2015.11.059.
[27] H. Zhang, T. Kuila, N.H. Kim, D.S. Yu, J.H. Lee, Simultaneous reduction, exfoliation, and nitrogen doping of graphene oxide via a hydrothermal reaction for energy storage electrode materials, Carbon. 69 (2014) 66–78. doi:10.1016/j.carbon.2013.11.059.
[28] B. Song, J. Zhao, M. Wang, J. Mullavey, Y. Zhu, Z. Geng, D. Chen, Y. Ding, K. Moon, M. Liu, C.-P. Wong, Systematic study on structural and electronic properties of diamine/triamine functionalized graphene networks for supercapacitor application, Nano Energy. 31 (2017) 183–193. doi:10.1016/j.nanoen.2016.10.057.

[29] D. Sun, X. Yan, J. Lang, Q. Xue, High performance supercapacitor electrode based on graphene paper via flame-induced reduction of graphene oxide paper, J. Power Sources. 222 (2013) 52–58. doi:10.1016/j.jpowsour.2012.08.059.
[30] H. Yang, S. Kannappan, A.S. Pandian, J.-H. Jang, Y.S. Lee, W. Lu, Nanoporous graphene materials by low-temperature vacuum-assisted thermal process for electrochemical energy storage, J. Power Sources. 284 (2015) 146–153. doi:10.1016/j.jpowsour.2015.03.015.
[31] E.Y.L. Teo, H.N. Lim, R. Jose, K.F. Chong, Aminopyrene functionalized reduced graphene oxide as a supercapacitor electrode, RSC Adv. 5 (2015) 38111–38116. doi:10.1039/C5RA02578H.
[32] R. Kötz, M. Carlen, Principles and applications of electrochemical capacitors, Electrochimica Acta. 45 (2000) 2483–2498. doi:10.1016/S0013-4686(00)00354-6.
[33] R.A. Aziz, I.I. Misnon, K.F. Chong, M.M. Yusoff, R. Jose, Layered sodium titanate nanostructures as a new electrode for high energy density supercapacitors, Electrochimica Acta. 113 (2013) 141–148. doi:10.1016/j.electacta.2013.09.128.
[34] X. An, T. Simmons, R. Shah, C. Wolfe, K.M. Lewis, M. Washington, S.K. Nayak, S. Talapatra, S. Kar, Stable Aqueous Dispersions of Noncovalently Functionalized Graphene from Graphite and their Multifunctional High-Performance Applications, Nano Lett. 10 (2010) 4295–4301. doi:10.1021/nl903557p.
[35] H.M. Jeong, J.W. Lee, W.H. Shin, Y.J. Choi, H.J. Shin, J.K. Kang, J.W. Choi, Nitrogen-Doped Graphene for High-Performance Ultracapacitors and the Importance of Nitrogen-Doped Sites at Basal Planes, Nano Lett. 11 (2011) 2472–2477. doi:10.1021/nl2009058.
[36] S. Biswas, L.T. Drzal, Multilayered Nanoarchitecture of Graphene Nanosheets and Polypyrrole Nanowires for High Performance Supercapacitor Electrodes, Chem. Mater. 22 (2010) 5667–5671. doi:10.1021/cm101132g.
[37] Z. Weng, Y. Su, D.-W. Wang, F. Li, J. Du, H.-M. Cheng, Graphene–Cellulose Paper Flexible Supercapacitors, Adv. Energy Mater. 1 (2011) 917–922. doi:10.1002/aenm.201100312.
[38] T.Y. Kim, H.W. Lee, M. Stoller, D.R. Dreyer, C.W. Bielawski, R.S. Ruoff, K.S. Suh, High-Performance Supercapacitors Based on Poly(ionic liquid)-Modified Graphene Electrodes, ACS Nano. 5 (2011) 436–442. doi:10.1021/nn101968p.
[39] M.D. Stoller, S. Park, Y. Zhu, J. An, R.S. Ruoff, Graphene-Based Ultracapacitors, Nano Lett. 8 (2008) 3498–3502. doi:10.1021/nl802558y.

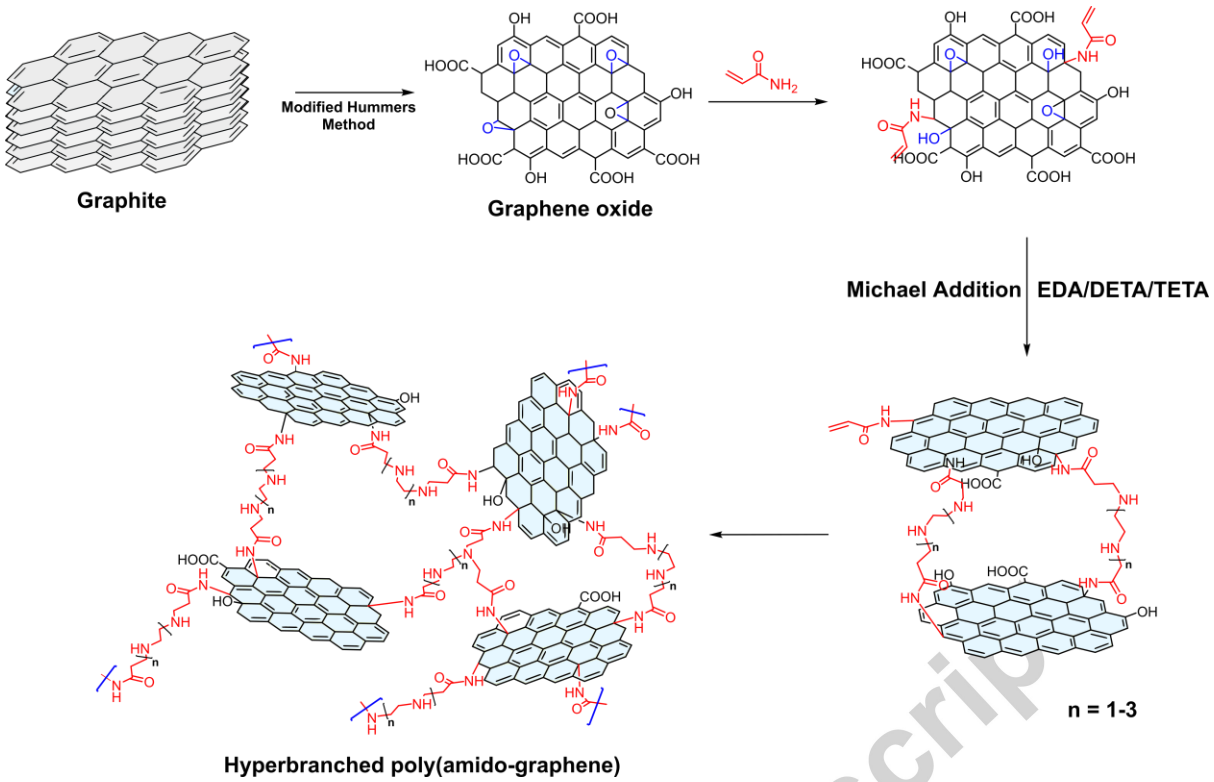

Figure 1. Schematic representation of synthesis of amine functionalized graphene oxide sheet (Scheme.1).

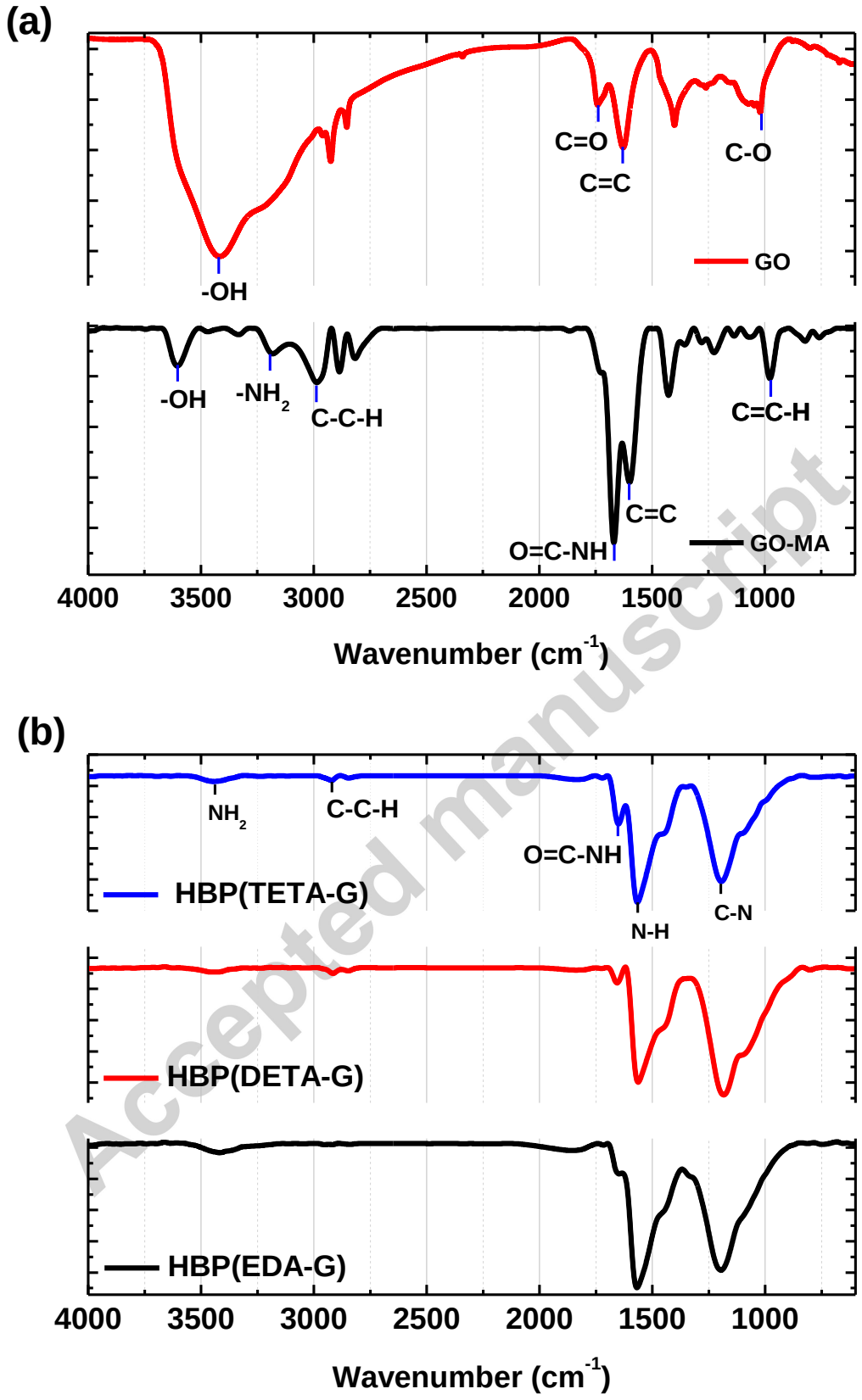

Figure 2. FTIR spectra of GO and GO-A; (b) HBP(EDA-G), HBP(DETA-G) and (HBP(TETA-G)

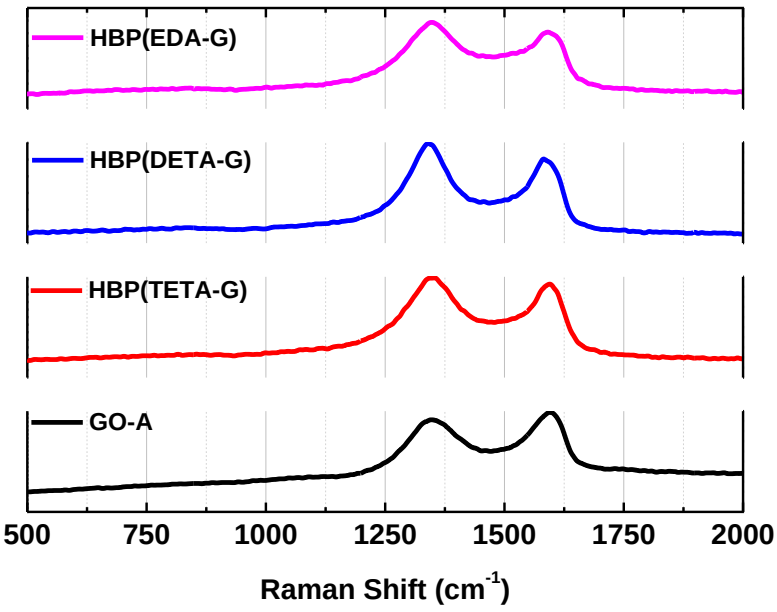

Figure 3. Raman spectra of GO-A, HBP(EDA-G), HBP(DETA-G) and HBP(TETA-G).

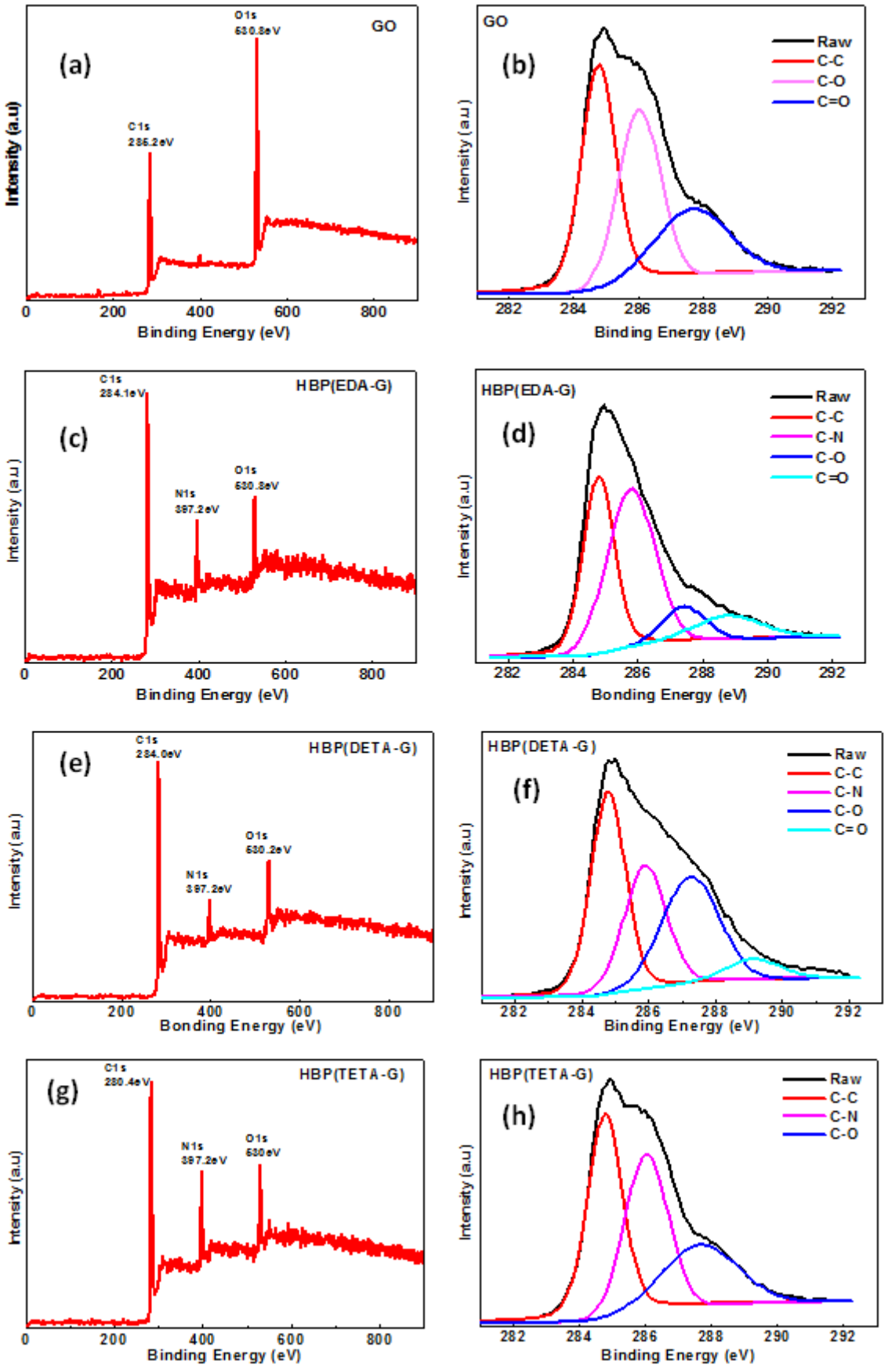
(a)
GO
O1s
530.8eV
C1s
285.2eV
Intensity (a.u)
Binding Energy (eV)
(b)
GO
Raw
C-C
C-O
C=O
Intensity (a.u)
Binding Energy (eV)
(c)
HBP(EDA-G)
C1s
284.1eV
N1s
397.2eV
O1s
530.8eV
Intensity (a.u)
Binding Energy (eV)
(d)
HBP(EDA-G)
Raw
C-C
C-N
C-O
C=O
Intensity (a.u)
Bonding Energy (eV)
(e)
HBP(DETA-G)
C1s
284.0eV
N1s
397.2eV
O1s
530.2eV
Intensity (a.u)
Bonding Energy (eV)
(f)
HBP(DETA-G)
Raw
C-C
C-N
C-O
C=O
Intensity (a.u)
Binding Energy (eV)
(g)
HBP(TETA-G)
C1s
280.4eV
N1s
397.2eV
O1s
530eV
Intensity (a.u)
Binding Energy (eV)
(h)
HBP(TETA-G)
Raw
C-C
C-N
C-O
Intensity (a.u)
Binding Energy (eV)

Figure 4. XPS spectra of synthesized graphene oxide derivatives (a) Survey spectra of GO; (b) C1s spectra of GO; (c) Survey spectra of HBP(EDA-G); (d) C1s spectra of HBP(EDA-G); (e) Survey spectra of HBP(DETA-G); (f) C1s spectra of HBP(DETA-G); (g) Survey spectra of HBP(TETA-G); and (h) C1s spectra of HBP(TETA-G).

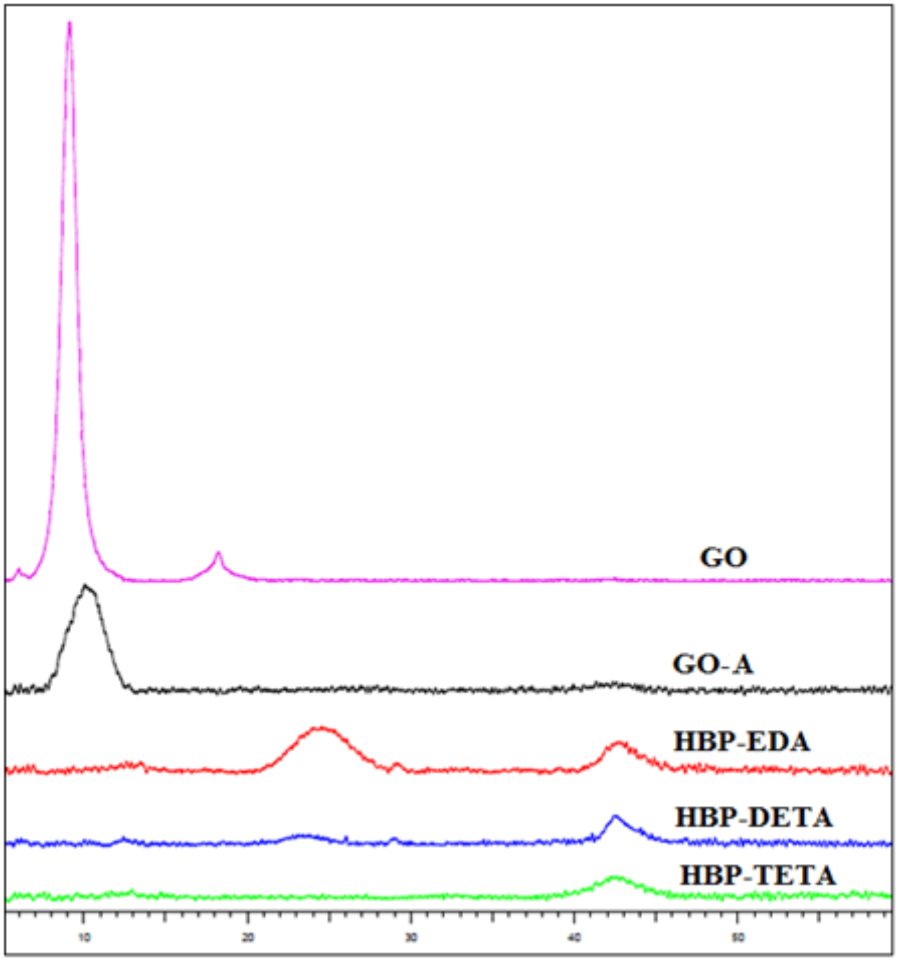

Figure 5. XRD spectra of GO, GO-A, HBP(EDA-G), HBP(DETA-G) and HBP(TETA-G)

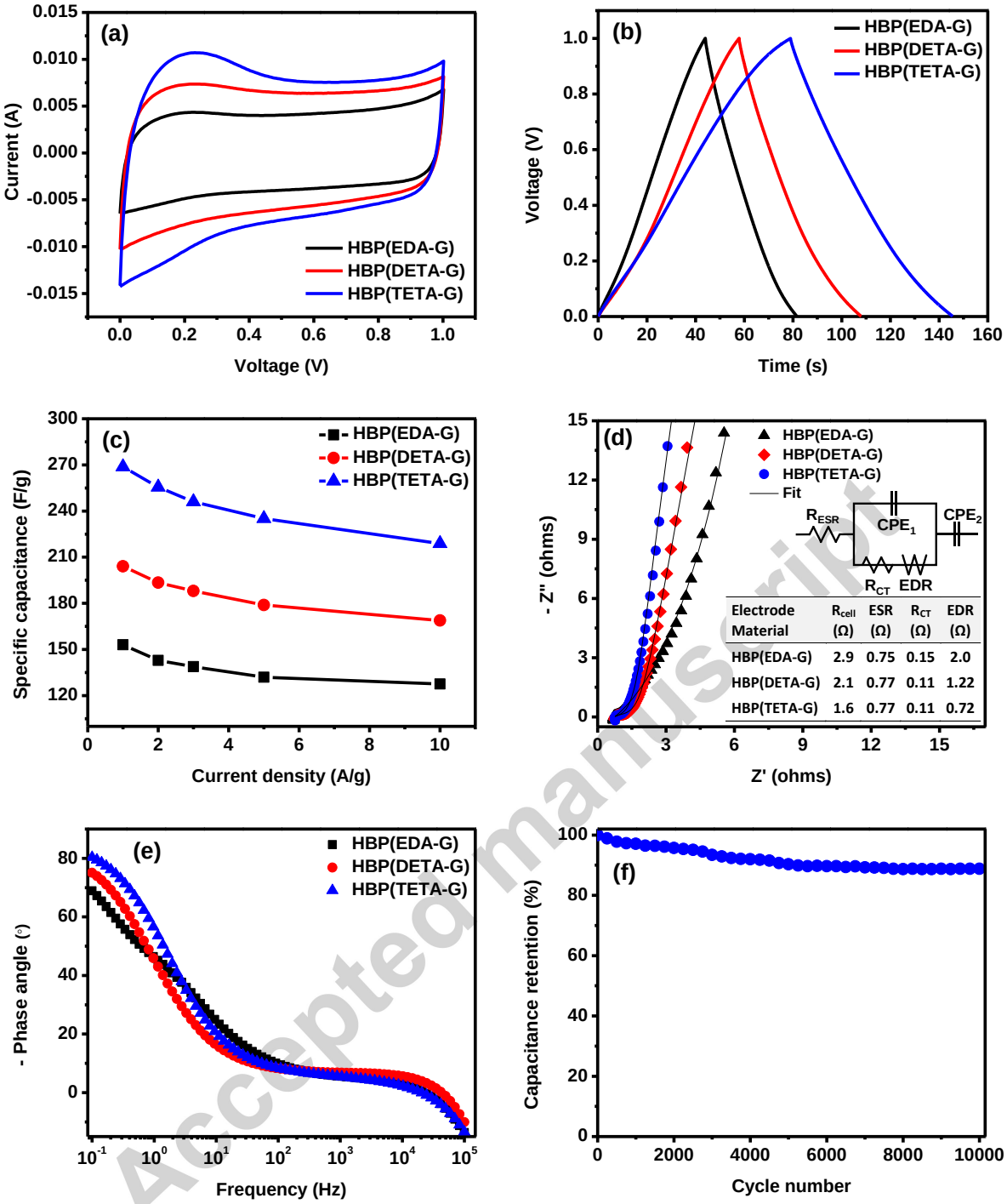

Figure 6. Electrochemical evaluation of HBP(EDA-G), HBP(DETA-G) and HBP(TETA-G) electrodes in 1M H_2SO_4 electrolyte (a) CV voltammogram at scan rate 100 mV/s between 0-1 V; (b) Galvanostatic charge/discharge curves at the current density of 1A g^{-1} between 0-1 V; (c) Specific capacitance values at as a function of current densities; (d) Nyquist plots, the lines indicate curve fitted as per the equivalent circuit given in the inset. Inset table lists the resistance of the components obtained by fitting the EIS curve to the equivalent circuit; (e) Bode plots; (f) Capacitance retention of HBP(TETA-G) electrode based supercapacitor cells over 10,000 cycling test between 0-1 V at current density of 10 A g^{-1}

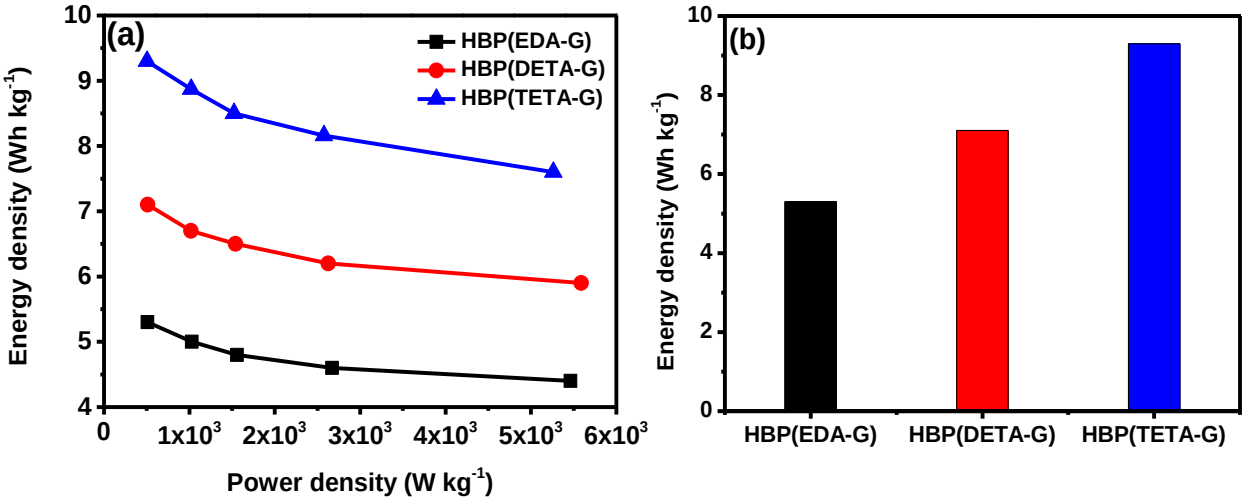

Figure 7. (a) Ragone plot of power density against energy density of HBP(EDA-G), HBP(DETA-G) and HBP(TETA-G); (b) Energy density of HBP(EDA-G), HBP(DETA-G) and HBP(TETA-G).

Table 1. Electrochemical performance of functionalized graphene based materials (two electrode method)

Materials	Electrolyte	Current density ($A\ g^{-1}$)	Specific capacitance ($F\ g^{-1}$)	Energy density ($Wh\ kg^{-1}$)	Reference
Noncovalent functionalized graphene	6M KOH	-	120	9.2	[34]
Nitrogen-doped graphene	6M KOH	1	282	-	[35]
Ap-rGO	6M KOH	-	160	5.6	[31]
PPy-graphene composite	1M NaCl	1	165	-	[36]
GCP	1M H_2SO_4	-	120	-	[37]
PIL-RG	EMIM-NTf_2	1	187	-	[38]
CMG	5.5M KOH	-	135	-	[39]
HBP(EDA-G)	1M H_2SO_4	1	153	5.3	This work
HBP(DETA-G)	1M H_2SO_4	1	204	7.1	This work
HBP(TETA-G)	1M H_2SO_4	1	269	9.3	This work

* Ap-rGO: Aminopyrene functionalized reduced graphene oxide; CMG: Chemically modified graphene; GCP: Graphene-Cellulose paper; PANI: Polyaniline; PIL-RG: Poly (Ionic liquid)-Modified Graphene; PPy: Polypyrrole.